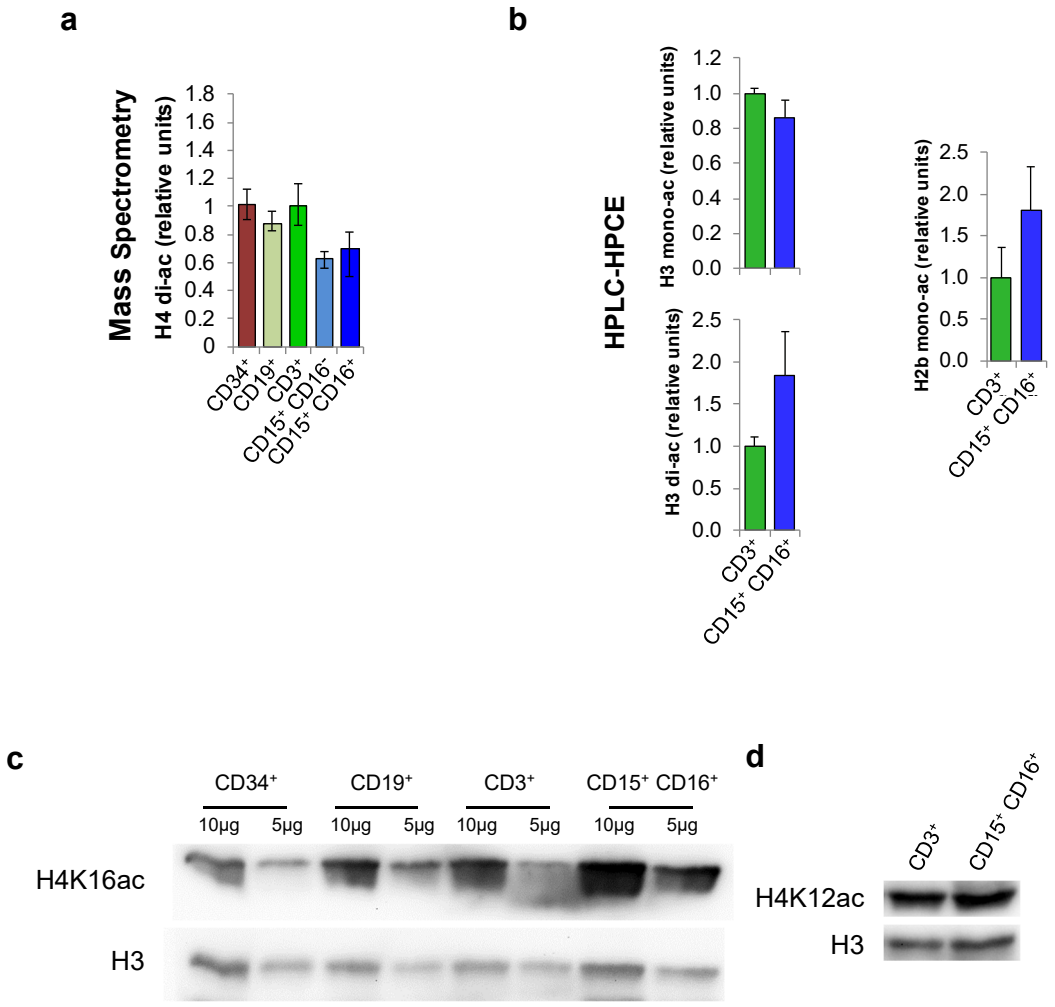

Supplementary Figure S1. Global acetylation levels in different types of blood cell. (a) Relative values of diacetylated isoforms of histone H4 analyzed by mass spectrometry (MALDI-TOF) in lymphoid versus myeloid populations. (b) Histone H3, and histone H2B global acetylation levels analyzed by HPLC and HPCE in neutrophils and $CD3^+$ T cells. (c) WB showing global levels of H4K16ac in the hematopoietic cells. Two dilutions of the cell lysates are shown. (d) WB showing no differences in H4K12ac between CD3+ T cells and neutrophils.

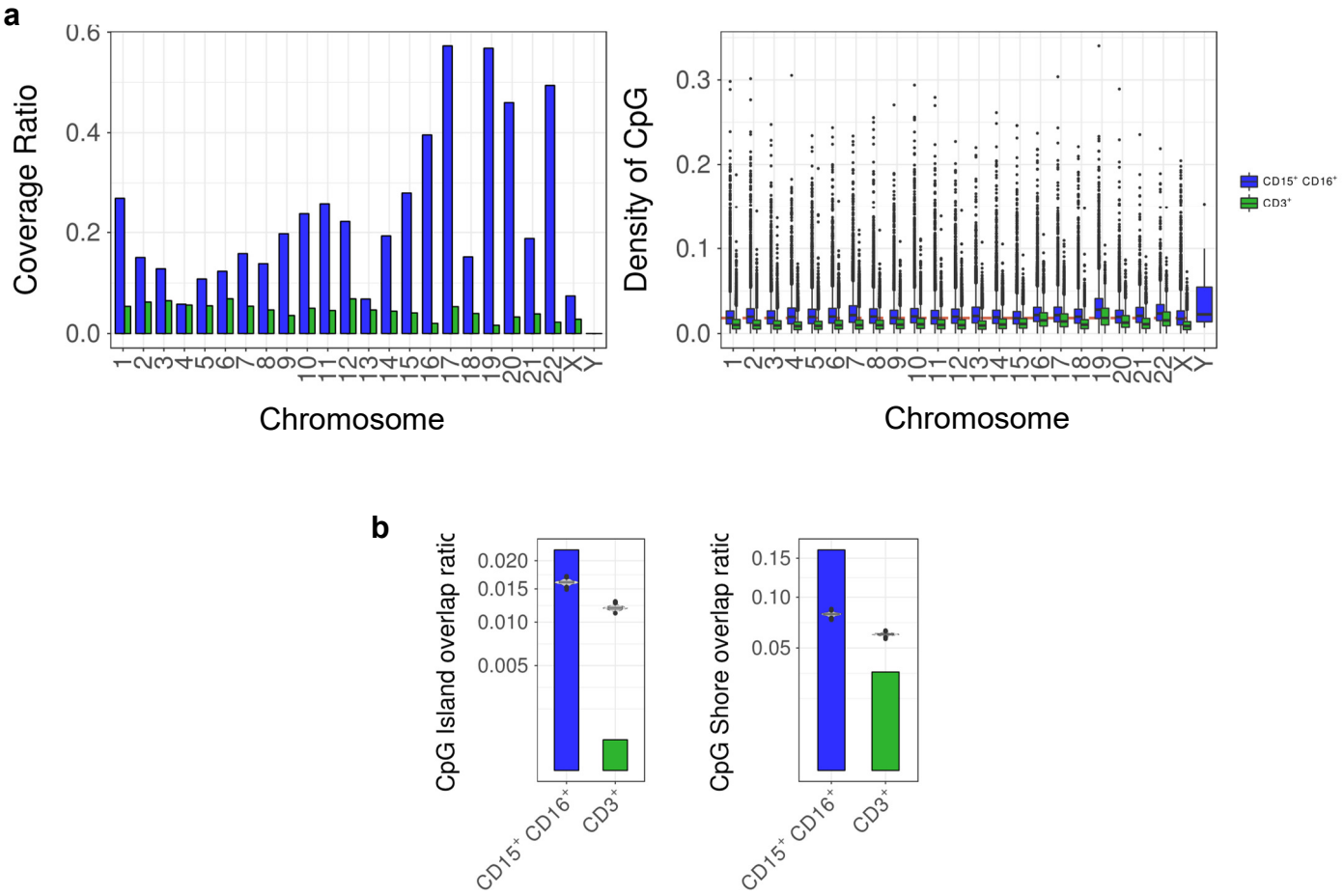

Supplementary Figure S2. Genomic distribution of H4K16ac. (a) Description of the H4K16ac-enriched peaks for each of the chromosomes related to the total coverage (in base pairs; bp) (left panel), and the distribution of CpG density (right panel), in neutrophils and $CD3^+$ T cells. Dotted red line represents average CpG density in the genome. (b) Bar plots showing the overlap between peaks with CpG islands (left panel), and with CpG shores (right panel). Violin plots represent a permutation-based null distribution for the CpG island overlap ratio for each peak data set.

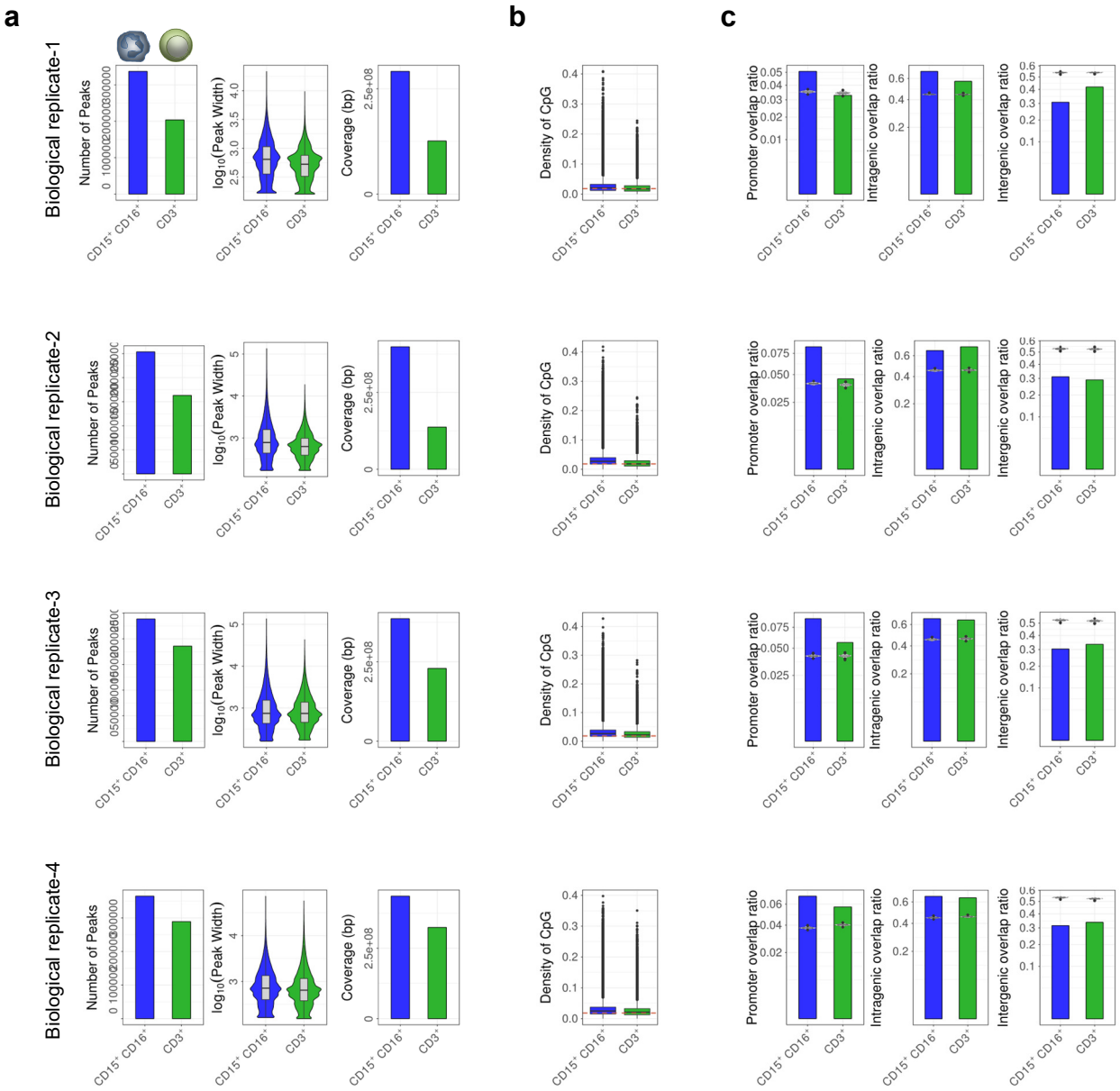

Supplementary Figure S3. Chip-seq validations in 4 additional independent biological replicates. (a) Bar plot showing the number of H4K16ac-enriched peaks identified by ChIP-seq in neutrophils and CD3$^+$ T cells. On the right, a violin plot shows the distribution of the peak size in both cell types, and a bar plot shows the total coverage of the genome in base pairs (bp). (b) Box plot showing the genomic distribution of CpG density for the H4K16ac-enriched peaks in both cell types. Dotted red line represents average CpG density in the genome. (c) Bar plots showing the overlap between H4K16ac-enriched peaks and different genomic regions in both neutrophils and T cells. Violin plots represent a permutation-based null distribution for the specific genomic region overlap ratio for each peak data set.

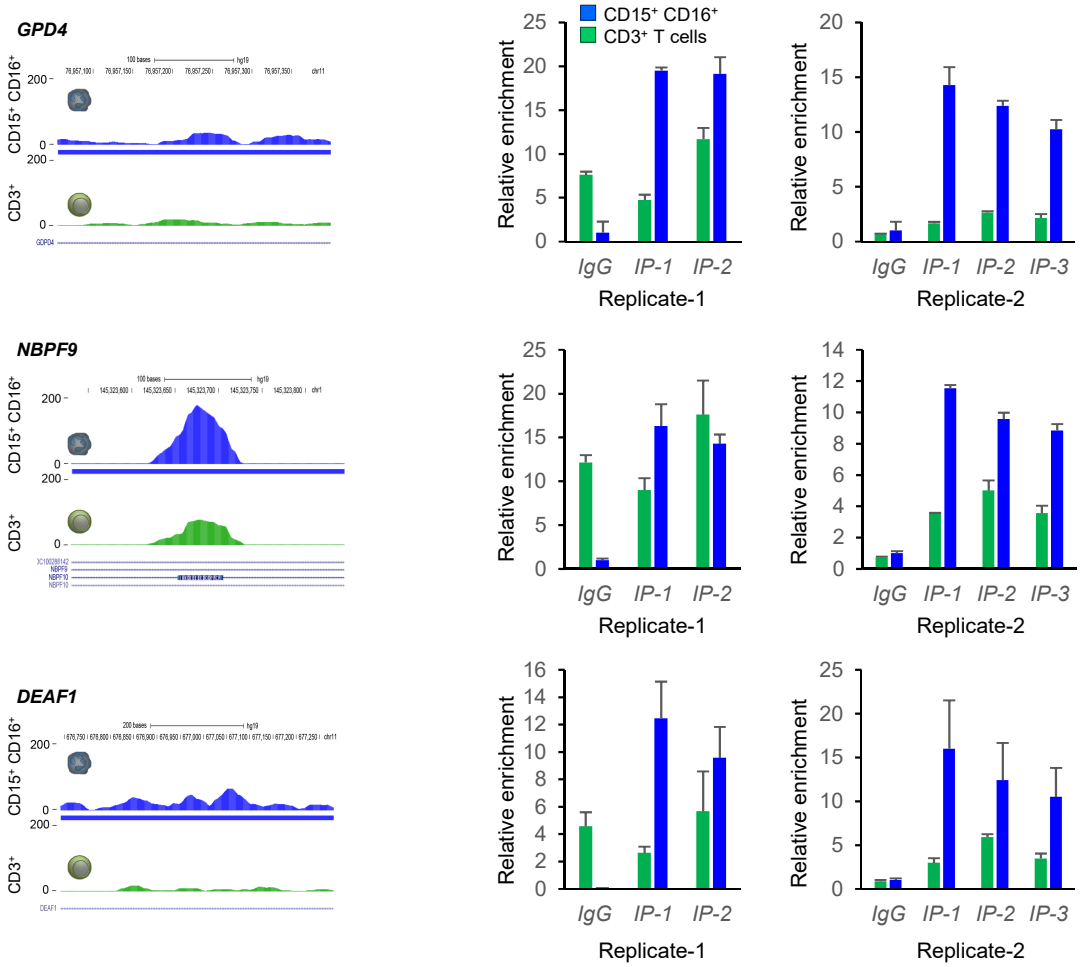

Supplementary Figure S4. ChIP-qPCR validations in neutrophils and CD3⁺ T cells in 2 independent biological replicates showing IgG and H4K16ac enrichment over several H4K16ac enriched-regions (genes) identified in the ChIP-seq assay. Ct values were transformed to quantities using the standard curve of each primer and, then, normalize to the IgG and the input. Data shown correspond to an average of triplicate measures (+SD). H4K16ac peaks identified by MACS2, and genome diagrams showing the relative enrichment of H4K16ac in neutrophils are shown on the left. Significant H4K16ac peaks showing fold change above 1.5 are indicated by a colored bar below the profile.

Supplementary Figure S5

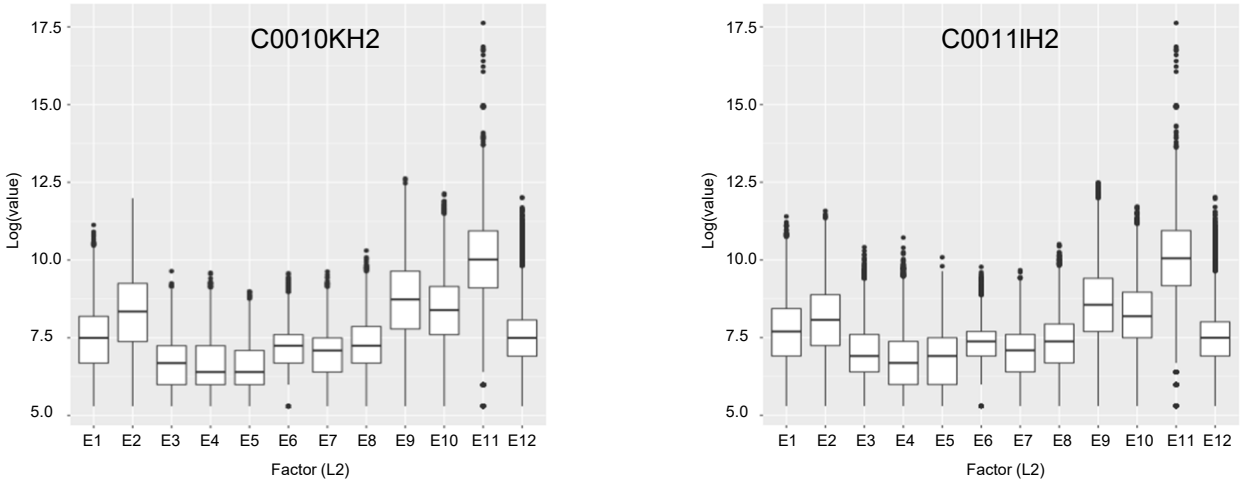

Supplementary Figure S5. Bar plots showing the size distribution of Chromatin states (named as in Figure 2f) for two neutrophil Blueprint samples (C0010KH2 and C0011IH2).

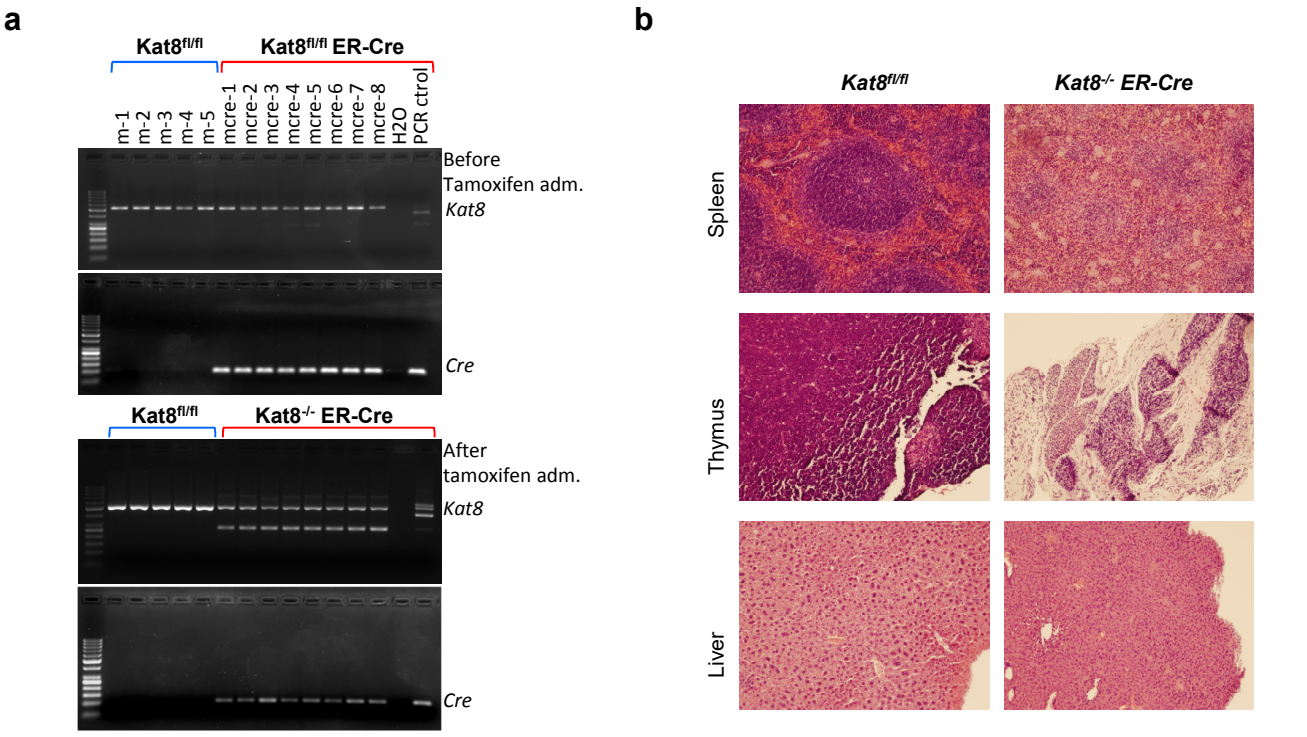

Supplementary Figure S6. (a) Tamoxifen-inducible Kat8 knockout mouse model. Genotype analysis of Kat8 and Cre loci by PCR specific primers using genomic DNA *from Kat8*$^{fl/fl}$ and *Kat8*$^{fl/fl}$*;ER-Cre* mice before (DNA from tail, upper panels), and after tamoxifen treatment (DNA from blood, lower panels). The double band indicating 50% aprox. excision of Kat8 was only detected in mice containing ER-Cre after treatment with tamoxifen (lower panel). This percentage of excision may be because all cells that deleted both / homozygous alleles die immediately. (b) Anatomopathological effects of *Kat8* depletion. Representative microscopic images of spleen, thymus, and liver from Kat8fl/fl and Kat8-/-;ER-Cre mice showing tissular alterations.

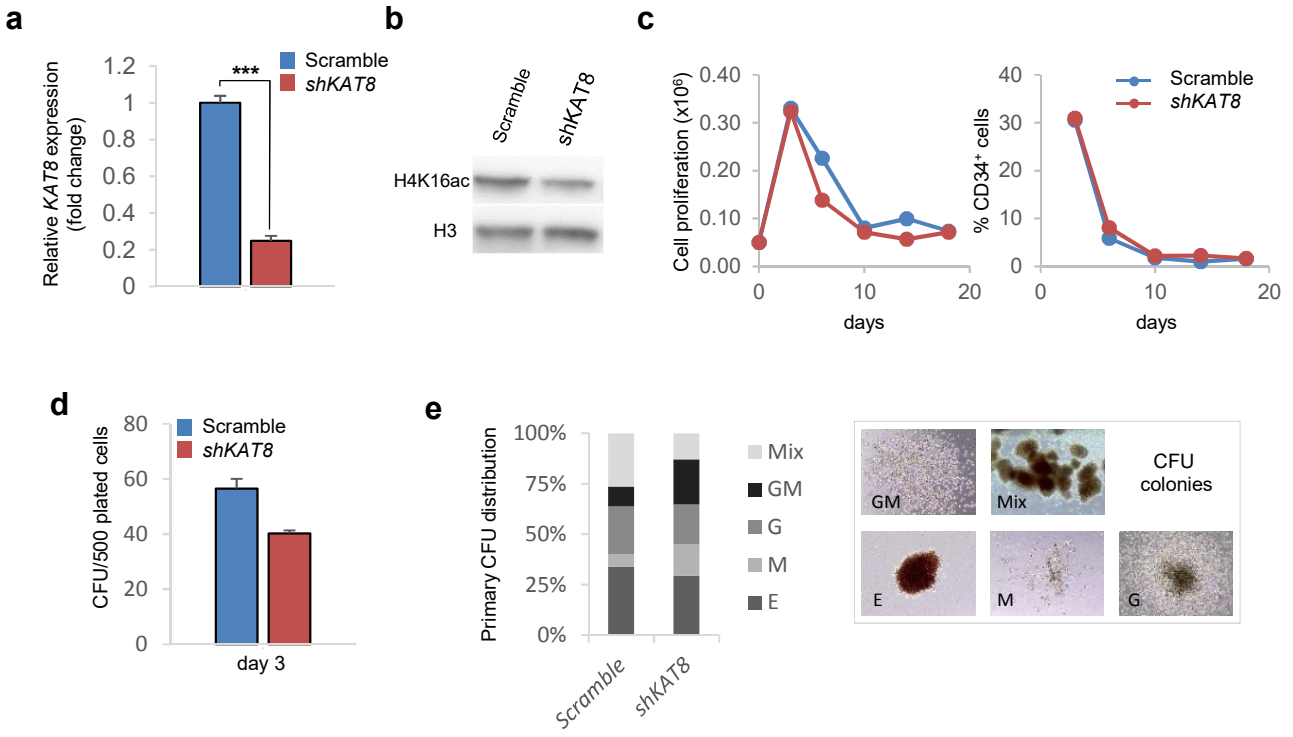

Supplementary Figure S7. (a) RT-qPCR showing downregulation of KAT8 in transduced human CD34⁺ progenitors in the clonogenic potential assay. Expression levels determined by real time-qPCR are an average of triplicated measurements (+SD), normalized to transcript levels of GAPDH, and represented as a fold-change relative to the scramble. (A t-test showed significant differences; ***: $p<0.001$) (b) WB showing an H4K16ac decrease in shKAT8 transduced cells. (c) Line plots showing the effects of shKAT8 on cell proliferation and the percentage of CD34+ progenitors during differentiation. (d) Bar-plot showing reduced hematopoietic potential (number of CFU per 500 cells seeded) in shKAT8 cells at day 3. (e) Stacked bars showing differences in distribution of CFU subtypes between CD34⁺ and shKAT8-transduced CD34⁺ cells. On the right there are representative images of different CFU subtypes, including erythroid (E), macrophage (M), granulocyte, (G) granulocyte-macrophage (G-M), and Mix, which contains a mixture of granulocytes, erythrocytes, megakaryocytes, and macrophages.

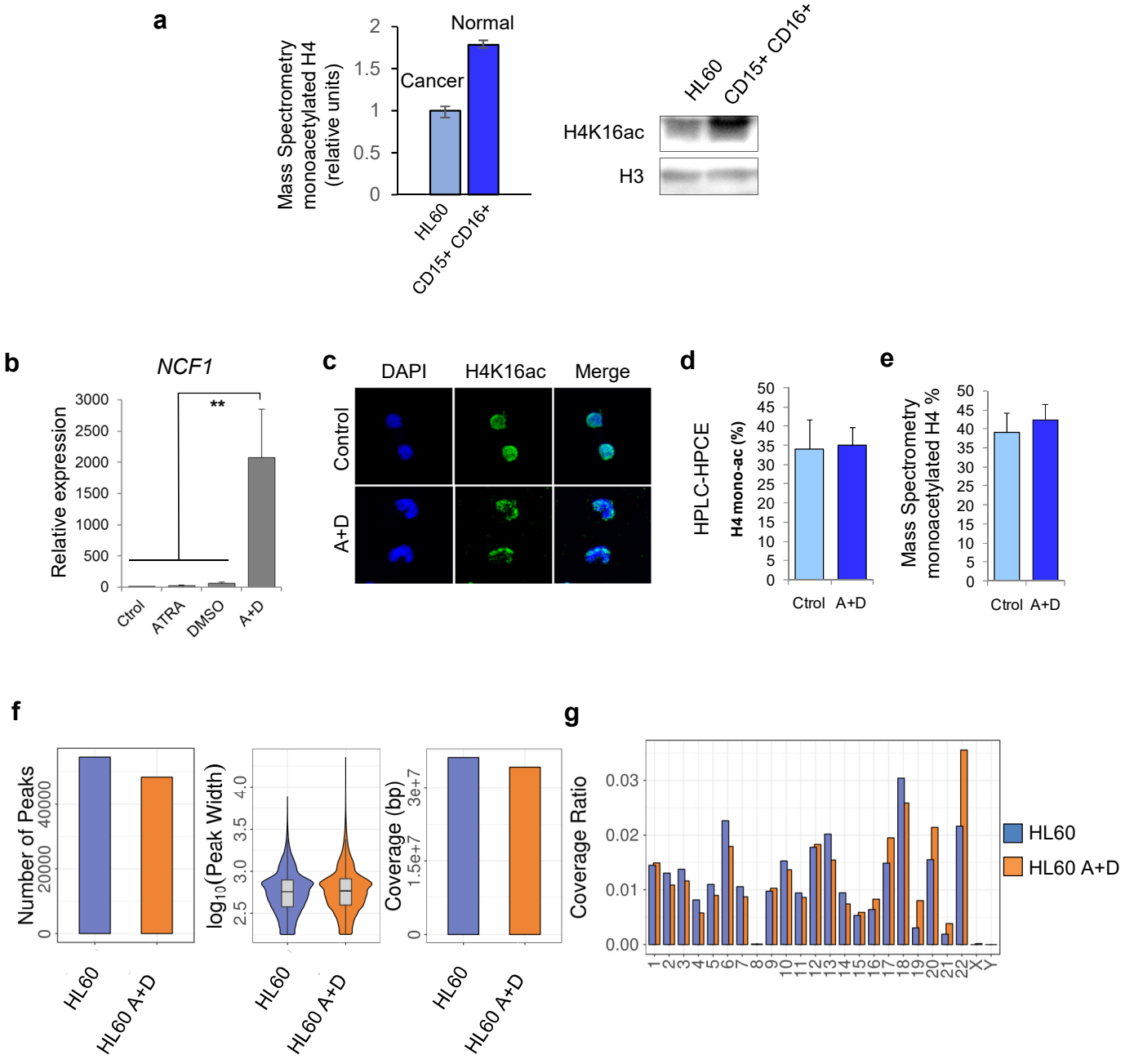

Supplementary Figure S8. (a) Global H4 monoacetylation analyzed by mass spectrometry and western blotting in HL60 cells and neutrophils. The error bars indicate the maximum and minimum values obtained from 6 spectra per sample (technical replicates). (b) Expression of NCF1 in HL60 cells using single and combined treatments with ATRA (A) and DMSO (D). Expression levels determined by real time-qPCR are an average of triplicated measurements (+SD), normalized to transcript levels of GAPDH, and represented as a fold-change relative to the control (A t-test showed significant differences; **: p<0.01). (c) Representative immunofluorescence staining of H4K16ac showing the multilobulated nuclear shape after combined treatment with A+D. (d) Global H4 monoacetylation analyzed by HPLC-HPCE, and by mass spectrometry (e). (f) Bar plot showing the number of H4K16ac-enriched peaks identified by ChIP-seq in HL60 and HL60 differentiated cells. On the right, a violin plot shows the distribution of the peak size in both samples, and a bar plot shows the total coverage of the genome in base pairs (bp). (g) Description of the H4K16ac-enriched peaks for each of the chromosomes related to the total coverage (in base pairs).

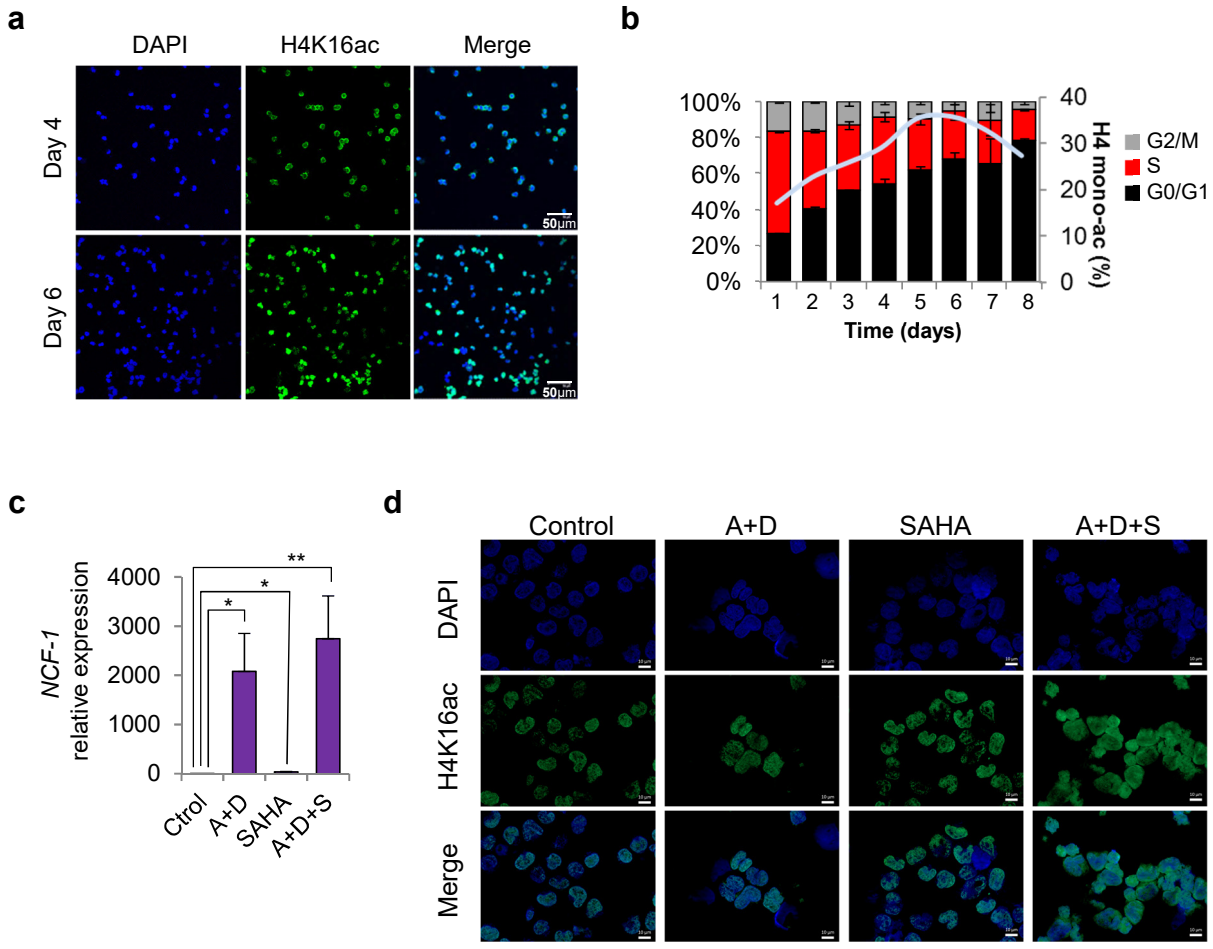

Supplementary Figure S9. (a) Immunofluorescences showing the changes in H4K16ac during the exponential growth of the cells at days 4 and 6. (b) Stacked bar plots showing the relationship between global H4K16ac (gray line) and each phase of the cell cycle during the exponential growth of the cells. (c) Expression levels of NCF1 as a marker of neutrophil differentiation in control and in vitro differentiated HL60 cells which were either untreated or treated with SAHA.). Expression levels determined by real time-qPCR are an average of triplicated measurements (+SD), normalized to transcript levels of GAPDH, and represented as a fold-change relative to the control (A t-test showed significant differences; *: $p<0.05$; **: $p<0.01$). (d) Representative immunofluorescence images showing levels of H4K16ac in the treatment with SAHA in control and HL60 differentiated cells. A: ATRA, D: DMSO, S: SAHA.

Supplementary Figure S10

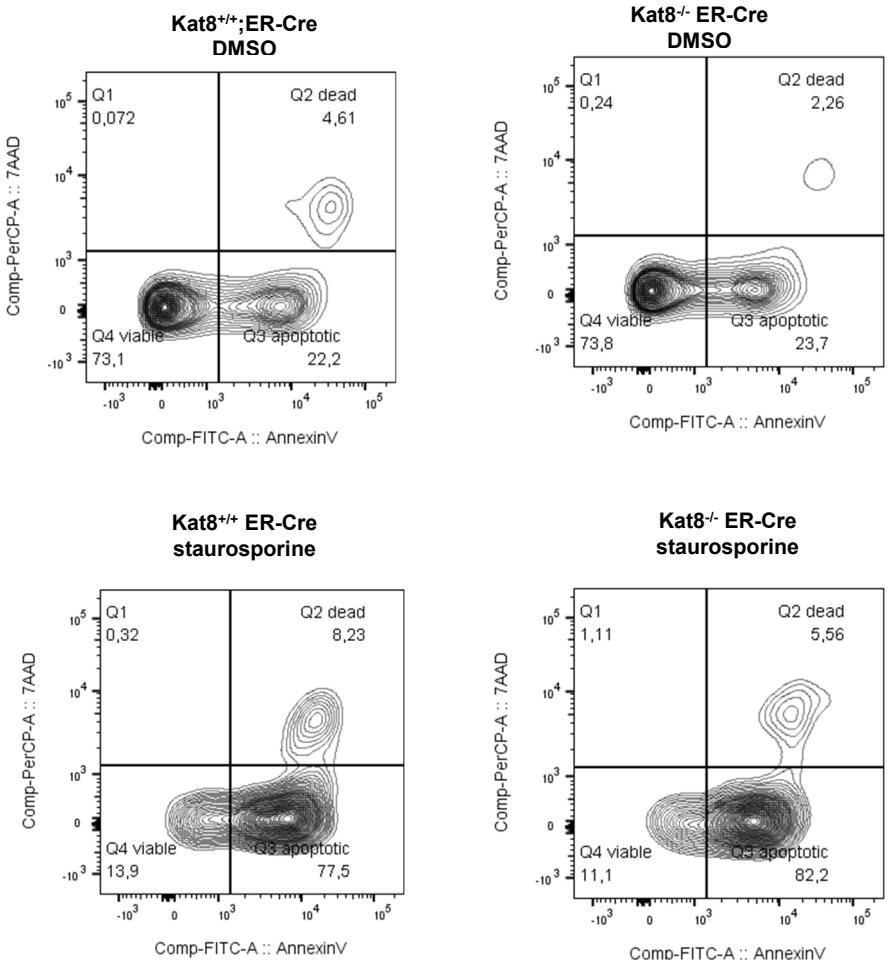

Supplementary Figure S10 . Levels of Annexin V-7AAD staining in cells derived from c-Kit+ differentiation to neutrophils at day 7 as determined by FACS.

Supplementary Figure S11

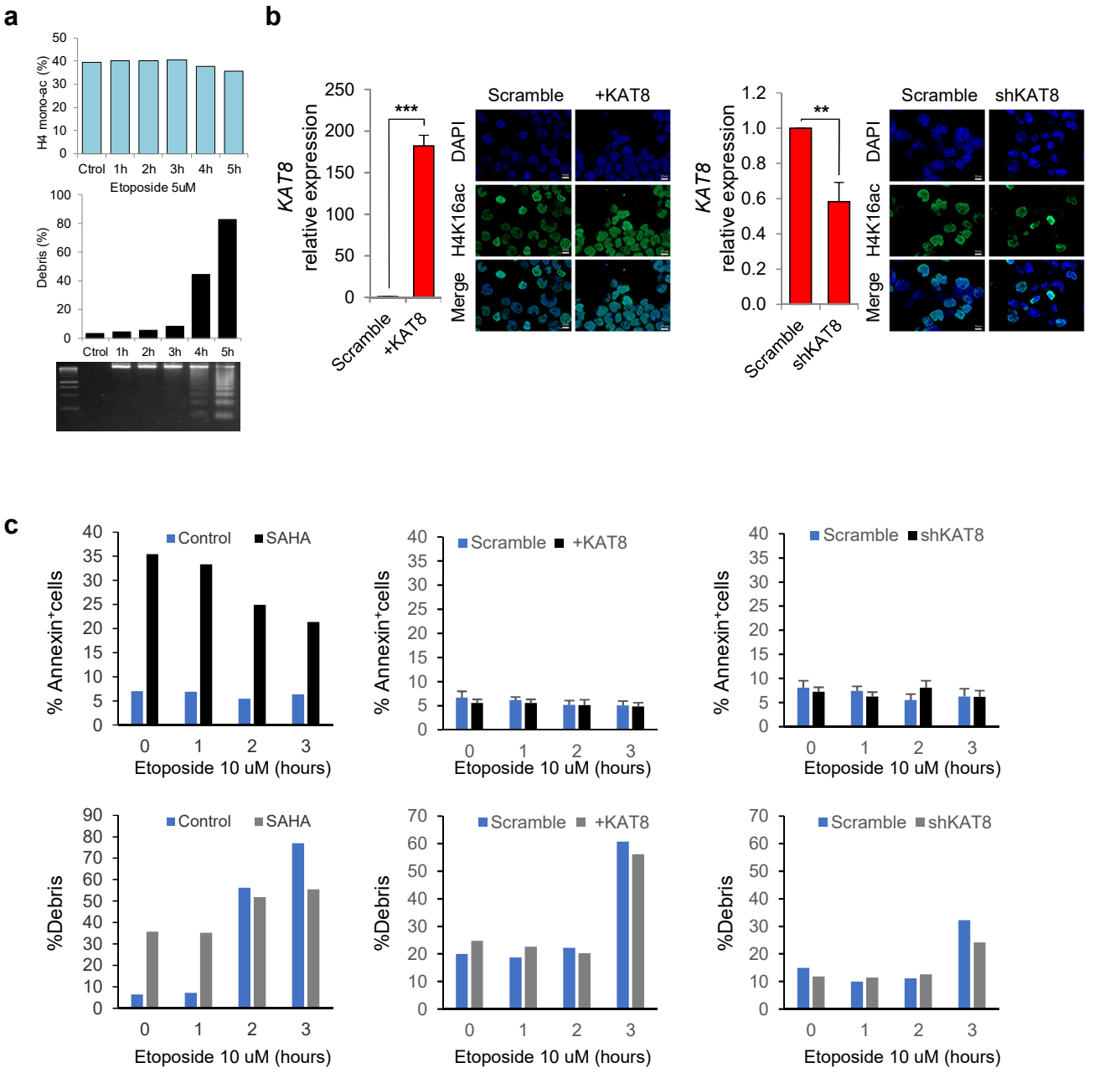

Supplementary Figure S11. (a) Global H4 monoacetylation analyzed by HPLC and HPCE (blue bars in the upper panel), and percentage of apoptosis measured by the percentage of debris in Propidium Iodide staining (lower panels) after the treatment of HL60 cells with the topoisomerase inhibitor etoposide.(b) Bar plots showing upregulation (on the left) and downregulation (on the right) of KAT8 in scramble and transduced HL60 cells. Expression levels determined by real time-qPCR are an average of triplicated measurements (+SD), normalized to transcript levels of GAPDH, and represented as a fold-change relative to the scramble (A t-test showed significant differences; ***: $p<0.001$; **: $p<0.01$). . Representative immunofluorescence images show levels of H4K16ac in these samples. (c) Bar plots showing the percentages of Annexin+ cells (upper panels) and debris (lower panes) during etoposide treatment of HL60 cells treated or not with SAHA (left panels), after *KAT8* upregulation (middle panels) and downregulation (right panels).

Supplementary Figure S12

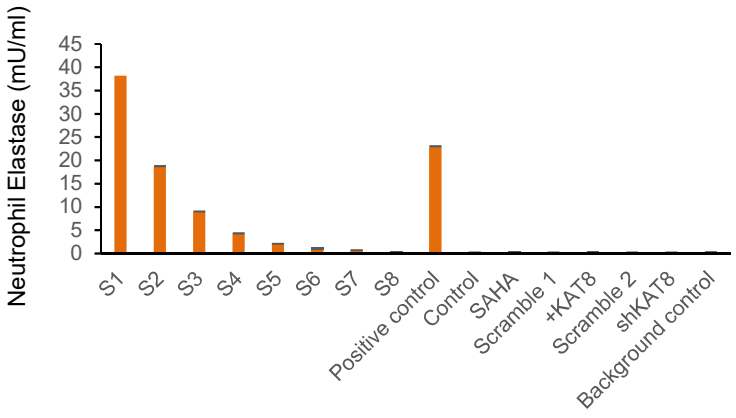

Supplementary Figure S12. Neutrophil elastase activity measurements from HL60 cells treated or not with SAHA as well as after the induction of up- or downregulation of *KAT8*. Results from standards (S1-S8), positive control and background control are also shown.

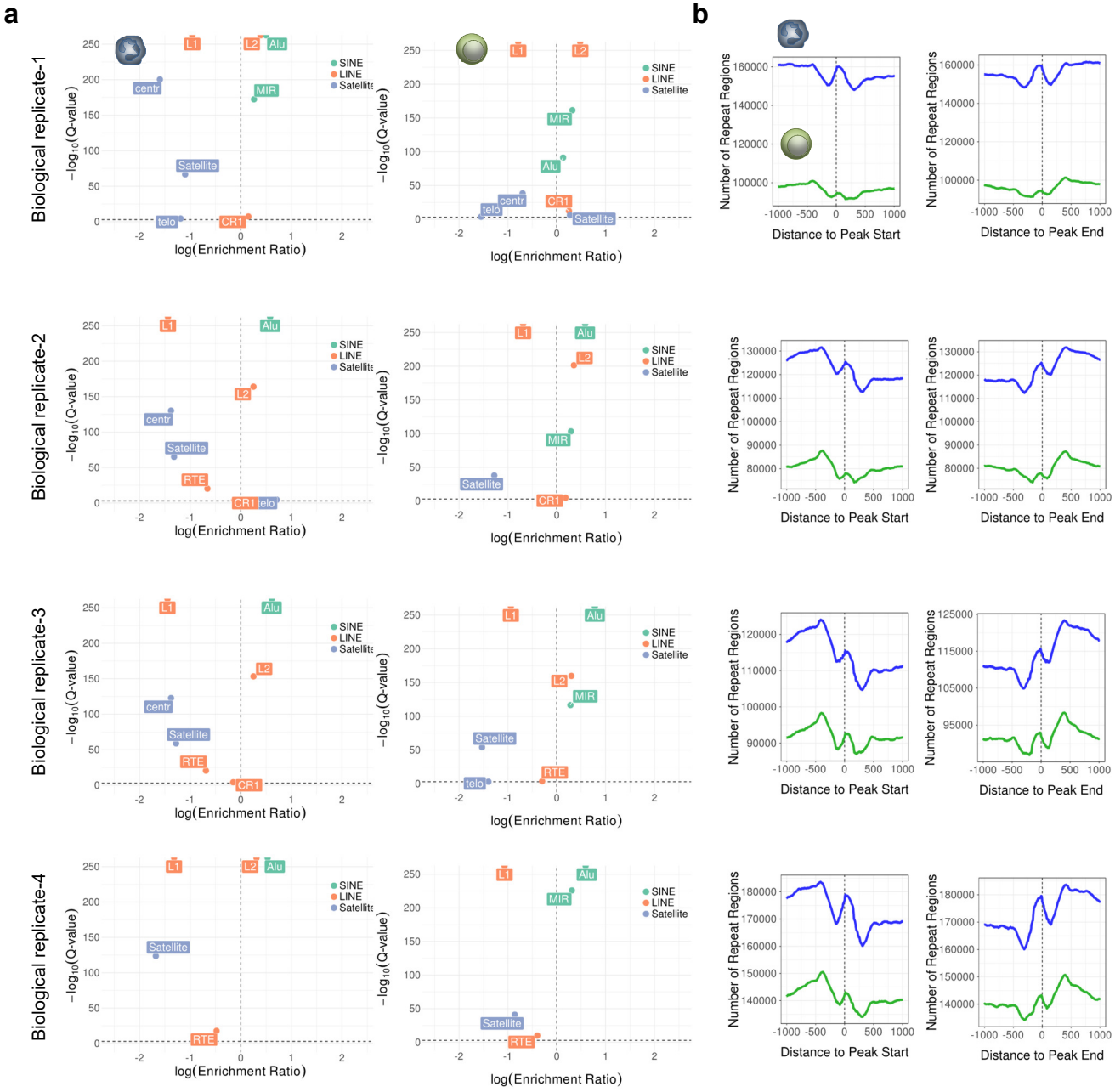

Supplementary Figure S13. Chip-seq validations in 4 additional independent biological replicates. (a) Enrichment analysis between different types of repetitive DNA elements with H4K16ac peaks (from the analyses of unique mapped reads) in neutrophils and $CD3^+$ T cells, ranked by Q-value, and enrichment score (relative risk). (b) Plots showing the coverage of repetitive elements in the regions flanking the H4K16ac enriched peaks obtained in the analyses of unique mapped reads in both cell types.

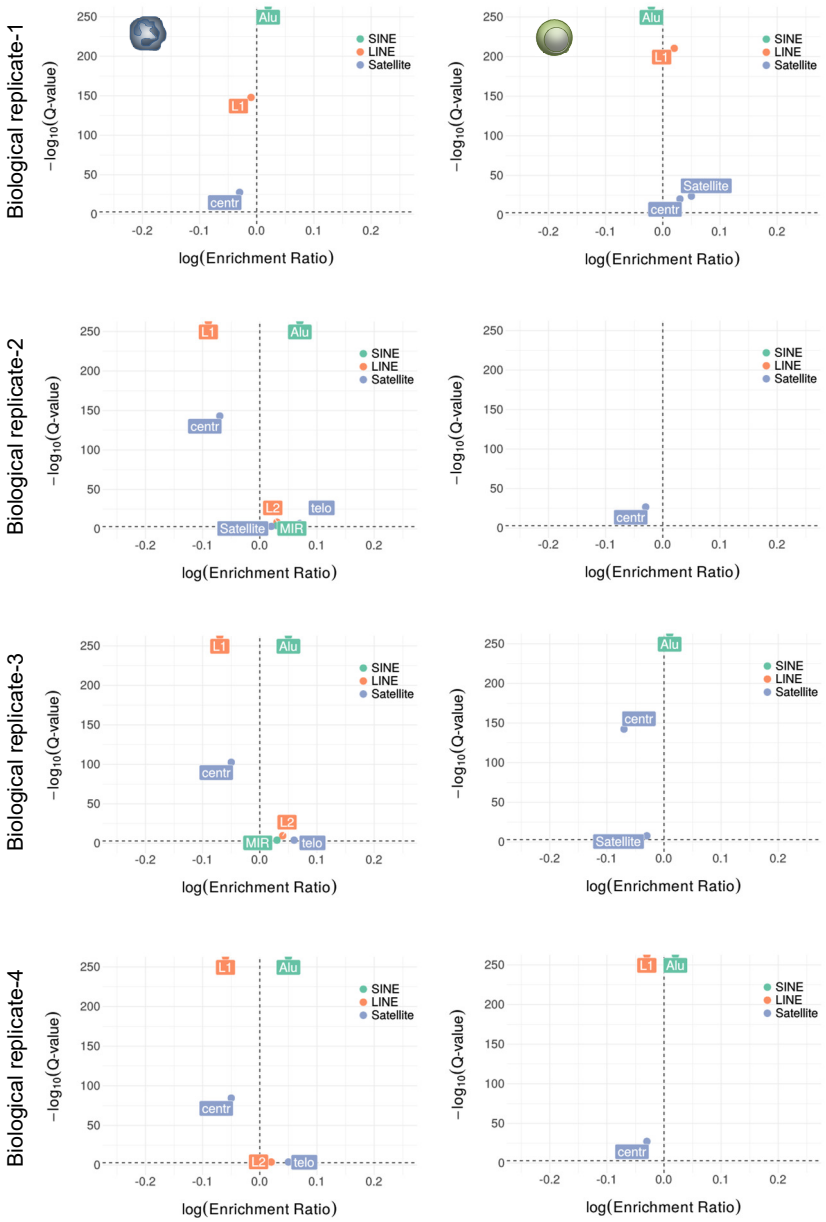

Supplementary Figure S14. Chip-seq validations in 4 additional independent biological replicates. Enrichment analysis between different types of repetitive DNA elements with probable H4K16ac-enriched regions (as indicated by their ambiguous mapping) in neutrophils and $CD3^+$ T cells, ranked by Q-value, and enrichment score (relative risk).

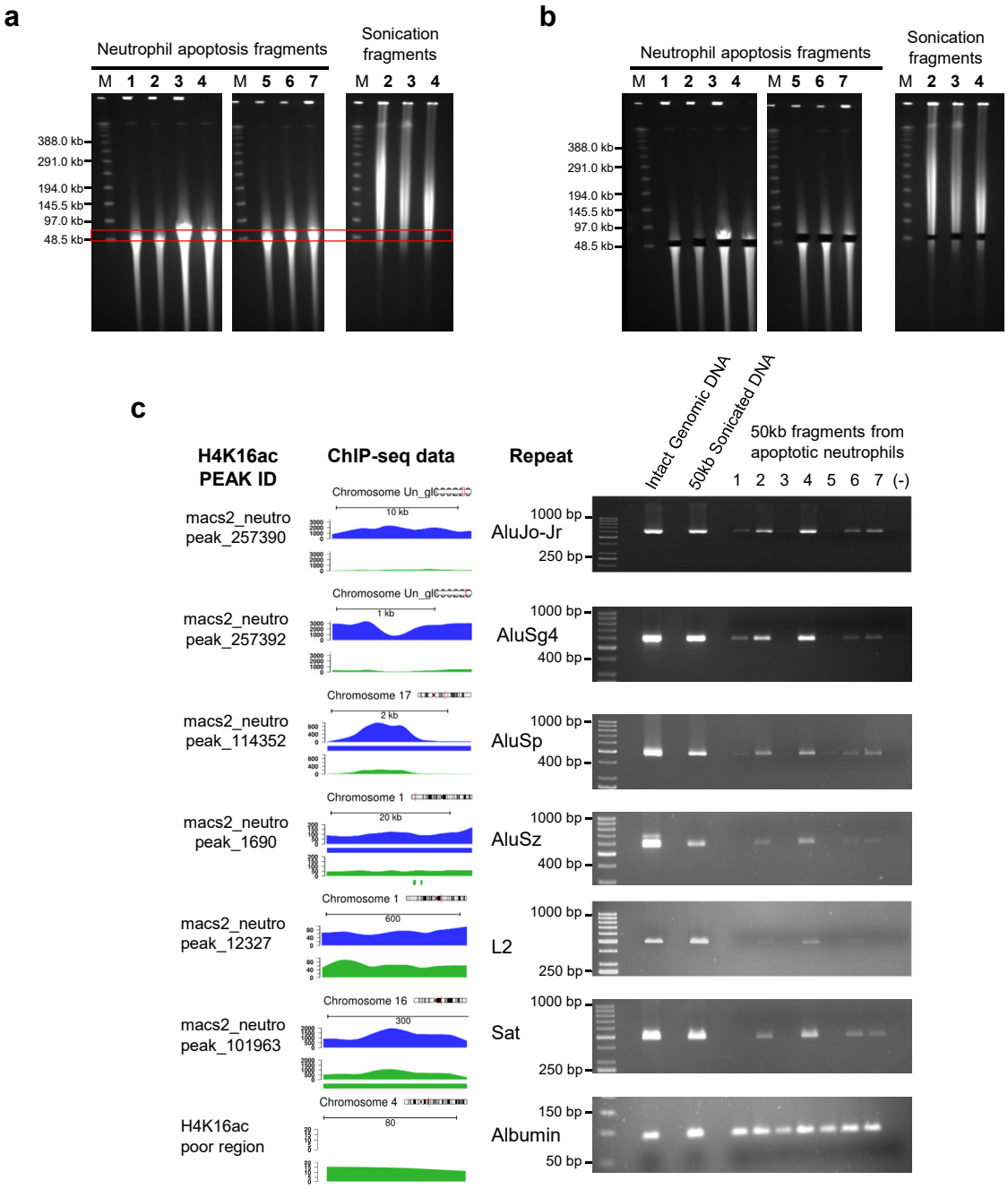

Supplementary Figure S15. Associations between H4K16ac-enriched regions and DNA breakage during neutrophil apoptosis. (a) PFGE of neutrophil apoptosis fragments from 7 healthy individuals (1-7). DNA from three individuals (2-4) fragmented randomly by sonication which were used as controls. 50kb DNA fragments are highlighted by a red frame. Lane M: DNA size marker. (b) Picture of the gel obtained from the PFGE taken after the 50Kb bands were excised for extraction and amplification of specific regions. (c) PCR amplification of specific DNA repetitive sequences using these same 50Kb DNA fragments. Genomic DNA and 50kb random fragments from a pool of samples were used as positive control. H4K16ac peaks identified by MACS2, and genome diagrams showing the relative enrichment of H4K16ac in neutrophils are shown on the left. Significant H4K16ac peaks showing fold change above 1.5 are indicated by a colored bar below the profile.

Supplementary Figure S16

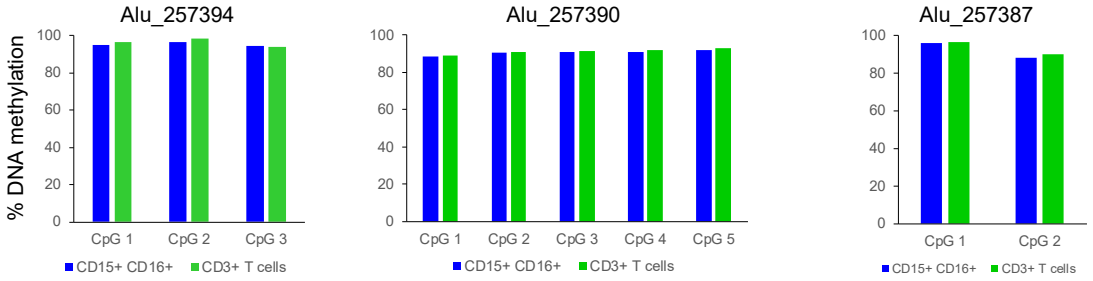

Supplementary Figure S16. Bar plots showing DNA methylation levels of three Alu repetitive sequences analyzed by bisulfite pyrosequencing in neutrophils and $CD3^+$ T cells.

Supplementary Figure S17

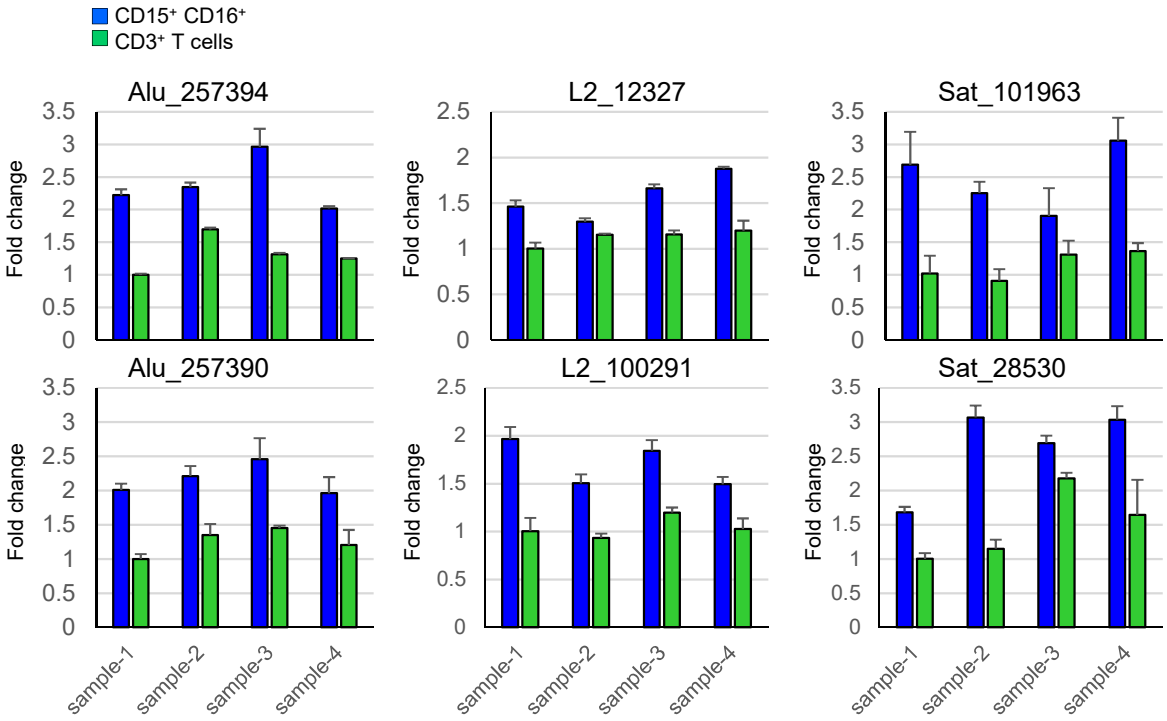

Supplementary Figure S17. qPCR amplification of enriched fragments from FAIRE assay showing that H4K16ac-enriched DNA repetitive sequences in neutrophils are more closely associated with open chromatin than in CD3+ T cells. Data are an average of triplicated measurements (+SD), normalized to a H4K16ac-poor region of the LOC126987 locus, and represented as a fold-change relative to the sample with the lowest value.

Supplementary Figure S18

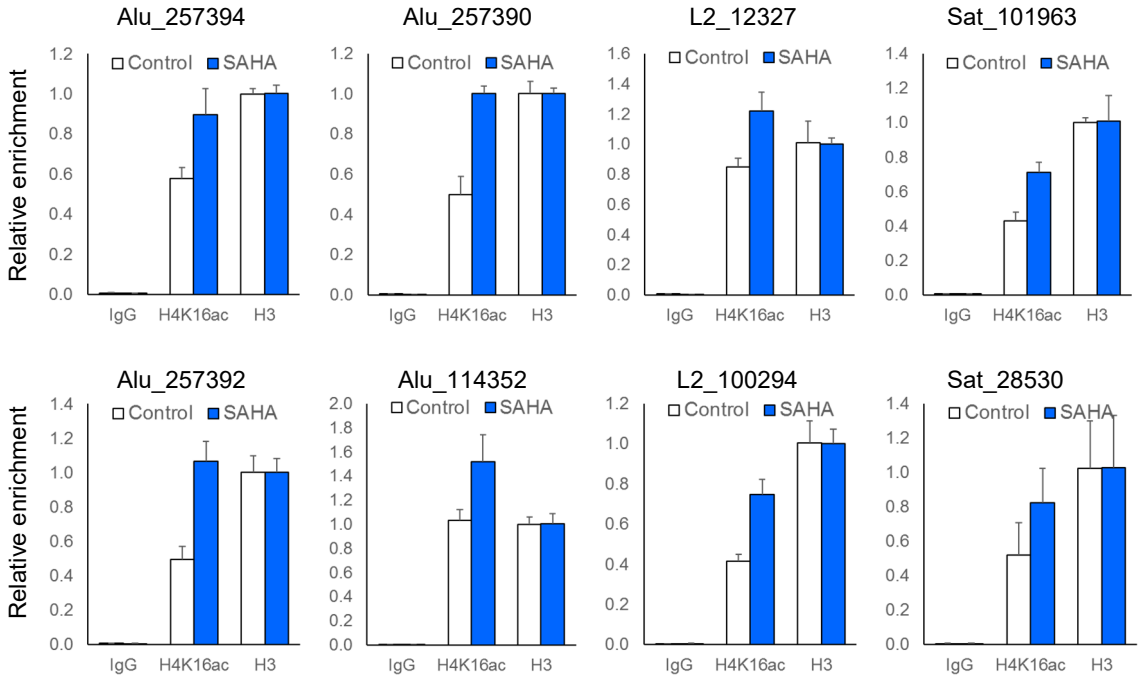

Supplementary Figure S18. ChIP-qPCR results in HL60 (white bars) and the same cancer cell line treated with SAHA (blue bars) showing IgG, H4K16ac, and H3 enrichment over several DNA repetitive sequences. Data are an average of triplicated measurements (+SD), normalized against H3.